The spatial resolution of micro-Raman spectroscopy for particulate $LiFePO_4$

Alexander A. Ryabin
Ural Federal University named after the first President of Russia B N Yeltsin: Ural'skij federal'nyj universitet imeni pervogo Prezidenta Rossii B N El'cina
Dmitry V. Pelegov (dmitry.pelegov@urfu.ru)
Ural Federal University named after the first President of Russia B N Yeltsin: Ural'skij federal'nyj universitet imeni pervogo Prezidenta Rossii B N El'cina https://orcid.org/0000-0002-0274-2572

Research Article

Keywords: penetration depth, probing depth, lithium iron phosphate, optical inhomogeneity, defects

Posted Date: February 15th, 2022

DOI: https://doi.org/10.21203/rs.3.rs-1313231/v1

Abstract

The fast-growing lithium battery industry needs quality control tools. Micro-Raman spectroscopy is a popular technique for structural characterization and impurity probing. The problem is that the method resolution can be appropriately quantified for a sample with planar geometry, like a single crystal, but not for a powder consisting of microparticles with irregular shape and surface. In this work, we have examined a series of single $LiFePO_4$ particles on a Raman-active Si substrate. This model experiment let us conclude that vertical resolution for particulate systems with inhomogeneity of shape and structure should be achieved be described not quantitative but qualitative. The observed variation of local probing depths is explained by spatial inhomogeneity of defects/impurities concentration, Mie scattering, blocking properties of pores, and surface plasmon resonance. In conclusion, we provide our recommendations for local and integral measurements using confocal Raman microscopy.

1. Introduction

Lithium iron phosphate $LiFePO_4$ (LFP) was introduced in 1997 as a candidate for cathode material in lithium batteries (from now on abbreviated as LB) [1,2]. During the following years, the LFP went through a series of twists and turns, from popularity in the early 2010s through a kind of oblivion in the late 2010s to a renaissance today [3]. LFP can be found in traction batteries for electric vehicles (buses, cars, trucks, etc.) [4–6], Starting-Lightning-Ignition batteries for gasoline cars [7], stationary energy storage solutions [8], and other energy storage products.

The electric vehicles and renewable energy industries are proliferating. To support their sustainable development, battery manufacturers should gradually build new manufacturing facilities worldwide and cut prices. Reducing costs, launching new production facilities in recent locations, and setting up new supply chains for raw materials can profoundly affect the quality of the final product. Raman spectroscopy (from now on abbreviated as RS) can be a cost-effective solution for low-cost quality control tools for both cathode material manufacturers and LB cell producer [6].

Progress in developing an RS-based quality control tool is hampered by the form of synthesized electrode materials – a powder consisting of micron and submicron particles. This is not specific only for the LB electrode materials, but it complicates the accurate description from a physical point of view. And the use of RS as a probing tool further complicates the characterization of microparticle systems.

A single crystal is the simplest object for accurate physical description, interpretation of experimental results, and theoretical calculations due to its regular structure and relatively simple formulation of boundary conditions. The presence of an imperfect surface layer complicates its description, but not much since bulk volume prevails over the surface one. In this case, RS can be considered a local tool due to the relatively small size of the probing laser spot.

At the opposite side of the scale bar, nanoparticles are also popular objects of physics research. It is unnecessary to study both bulk and surface since the entire volume of the studied object can be considered a surface. Raman probing of nanoparticles can be regarded as an integral measurement, averaging the responses over many particles. Due to their small size, the shape of these particles is often not considered. In some cases, it is possible to simplify a nanoparticle to a spherical object or even neglect particle size and treat the nano-particulate system as a continuous medium.

Microparticles typical of LB electrode materials fall somewhere between these two extreme cases, making them difficult to describe accurately. It contains both bulk and surface volumes. The particle size is comparable to the diameter of the probing laser beam; therefore, we cannot consider a particle either as infinitely large (local RS-probing) or as infinitesimal (integral RS-probing). Complex shapes usually characterize particles a few microns in size; therefore the geometric description of the interaction of the laser beam with the particle surface, as well as the correct determination of the boundary conditions, becomes difficult. Since the studied volume is not large, the thermodynamic description of the physical processes in such a micron-scale particle is dubious. How to research powder samples being so difficult to describe physically?

The correct interpretation of RS measurements for LB electrode materials should address all the issues mentioned above and many others. This article aimed to find answers to only one question, but we hope this will help in the proper interpretation of the measured Raman spectra. The question is estimating the RS spatial resolution for particulate electrode materials. It was conceived in 2006 by Julien et al.[9]. The authors mention about RS probing that *"Since the penetration depth of the light inside the $LiFePO_4$ particles in Raman scattering is very small, this technique is a probe of the first layers at the surface of coated particles, and allows the detection of carbon coating"* [9]. These words are illustrative as the authors are some of the most prolific researchers reporting on the RS characterization of LB materials.

Even though the authors studied the particles with a carbon coating, the RS probing volume in both pristine and carbon-coated electrode materials is still unclear. At the same time, the estimation of both vertical and lateral resolution (Δz and R correspondingly) is essential for the proper interpretation of the Raman spectra of particulate samples, especially those measured using Micro-Raman spectroscopy (μRS in short). The focus of this paper is on the vertical μRS resolution, or in other words, the μRS probing depth. Let's distinguish three possible cases, schematically illustrated in Figure 1:

1. the Raman spectrum is measured superficially and contains comparable responses from both the surface and the bulk of the particle under study (Fig. 1a).
2. the entire particle is probed, and the response from the bulk prevails over the response from the surface (Fig. 1b).
3. the Raman spectrum contains responses both from the directly probed particle and from other particles located under it (Fig. 1c).

μRS is a well-developed method, and estimates of its spatial resolution can be found in many publications [10–17]. The issue that we address in this work is to understand to what extent theoretical estimations made mainly for single crystals are suitable for such a complex object as a powder with particle size close to the wavelength of the probing laser radiation. These particles are irregular in shape and contain various defects, complicating the accurate theoretical description. This experimental study of spatial resolution in a particulate system is crucial for accurately interpreting measured Raman spectra and its use as quality control tools for electrode materials.

2. Materials And Methods

2.1. Studied materials

Samples were provided by partner research groups. Vadim S. Gorshkov and Artur R. Makhmutov synthesized the pristine LiFePO4 sample using a solid-state procedure from chemically pure ferrous oxalate dihydrate $FeC_2O_4 \cdot (H_2O)_2$ and chemically pure lithium metaphosphate $LiPO_3$ in five stages, each of which consisted of annealing in an argon atmosphere and subsequent grinding of the reaction products. The carbon-coated $LiFePO_4$ was provided by the team of Prof. Jongwoo Lim (Department of Chemistry, Seoul National University, Korea). 10 wt.% of sucrose powder was mixed with LFP active powder to pyrolyze the carbon coating.

2.2. Equipment

Raman spectra were measured in the ambient atmosphere using a confocal Raman microscope Alpha 300 RA (WiTec GmbH, Germany) with a 633-nm He-Ne laser source and a 100× lens with NA = 0.75. The scattered light was collected in a backscattering geometry and passed through an edge filter. Multimode optical fiber with a diameter of 50 μm was used as a confocal pinhole. A diffraction grating with 600 grids per millimeter and a 1600 pixels wide CCD camera provided spectral resolution about 2.1 cm^{-1} at 50 cm^{-1} and 1.7 cm^{-1} at 1100 cm^{-1}. The probing laser power was set at 1.5 mW by adjusting the diameter of the incoming laser beam using a built-in screw and measuring the power directly in the output beam by laser power and energy meter Vega with photodiode laser sensor PD300R-3W (Ophir Photonics, Israel). Scanning electron microscope (SEM) images were obtained using a Merlin workstation (Carl Zeiss, Germany) with an electron beam generated by a Schottky field emission gun.

2.3. Methods and approaches

2.3.1. Particle deposition

In this research, we used dry deposition and gentle distribution of LFP powder on a Raman-active silicon substrate followed by a dry air purge to remove aggregates. The Si substrate used was tagged with a DAD3220 (Disco) automatic dicing saw to provide unambiguous identification of the particles' locations, allowing repeated measurements and a combination of SEM imaging and RS characterization for any given particle.

2.3.2. Manual and automated measurements

To ensure reproducible positioning of the probing laser beam relative to the LFP particle under study, two alternative positioning methods were used: manual and automated. In both cases, the initial positioning of the probing laser beam in the X-Y plane was performed using an optical system. Preliminary positioning in the Z direction was made using the optical system by adjusting the maximum optical contrast for the particle under study.

In the case of manual positioning, the oscilloscope mode was used with 1 s averaging. The position of the laser beam relatively LFP@Si particle was adjusted in real-time by a piezo-driven scan stage: first along the X-axis, then along the Y-axis, and finally along the Z-axis to obtain the highest ratio of the 950 cm^{-1} LFP band relatively 520 cm^{-1} Si band. Thus, the resulting position was considered the point with the greatest contribution from the LFP. This manual method proved to be effective for particles smaller than 1.25 μm in diameter. In this case, the average measurement time was about 2.5 minutes per particle.

In the case of larger particles with a diameter of more than 1.25 μm, manual positioning was lingering; therefore, automated two-step positioning has become the preferred choice. At the first step, we found the position of the highest ratio of the 950 cm^{-1} LFP band to the 520 cm^{-1} Si band in the X-Y plane using standard built-in image scanning mode. At the second step, we moved to the found point and scanned in the Z direction. This semi-automatic positioning took about 7-9 minutes and required a manual transition between X-Y and Z scans. Fully automated positioning using 3D mapping can be also used, but this fully automated procedure will take even longer (tens of minutes).

A total of 72 particles were measured. For 32 particles, only manual positioning was used, for 31 – only automatic positioning, and 9 particles were measured using both manual and automatic techniques. Comparing these two alternative techniques for the same particles led to the conclusion that these two positioning methods gave almost the same result.

2.3.3. Particle size estimation

In this work, we used a simplified procedure for estimating the size of irregularly shaped particles from their area. Using the SEM image for every single particle studied, we calculated its area in the X-Y projection (hereafter referred to as S). First, S was found in pixels using the standard Adobe Photoshop selection tool (this can also be done using alternative software). Next, we determined the pixel size for the given SEM image and converted S to square nanometers. Finally, the estimated diameter D_{es} was defined as:

$$D_{es} = 2 \cdot (S/\pi)^{1/2} \quad (1)$$

D_{es} refers to the particle size in the XY plane, while the particle height (size in the Z direction) is expected to be smaller, but not much.

3. Results And Discussion

3.1. Some theoretical estimations of μRS probing depth

There are several ways to estimate the μRS probing depth, which is commonly mentioned in literature. Light attenuation by free charge carriers is mainly used for conductors but is also suitable for a poorly conducting material such as LFP. The light penetration δ, in this case, can be estimated as [18]:

$$\delta = 2 \cdot \sigma^{-1} \cdot (\varepsilon / \mu)^{1/2} \quad (2)$$

where σ is the electrical conductivity, ε and μ are the relative permittivity and the relative permeability respectively. For LFP with σ about 10^{-9} S/cm [19], δ is too large and even the growth of electronic conductivity by orders of magnitude due to doping or defects [20] keep it far above microns.

Light attenuation by optical absorption due to promoting transitions between electronic states of the material is another factor, limiting probing depth [21]. In this case, the $\delta_{absorption}$ is defined by absorption coefficient γ dependent on the photon frequency υ:

$$\delta_{absorption} \sim \gamma(\upsilon)^{-1} \quad (3)$$

Unfortunately, there is a lack of publications quantifying the absorption coefficient γ for LFP powder. Since LFP is a transparent material used in electrochromic devices and translucent batteries [22–24], the absorption coefficient is expected to be low but the local variations of defects and surface roughness can increase it, thus decreasing the probing depth.

Probing depth quantification by “Airy disk” is possibly the most popular approach for instrumental resolution estimations and commonly attributed to a theoretical limit of probing laser radiation focusing in the air (vertical component) [15]:

$$\Delta z = \lambda / NA^2 \quad (4)$$

where λ is the laser wavelength and NA is the numerical aperture of the microscope objective in air. In our case Δz is about 1.1 μm (for λ = 0.633 and NA= 0.75). Due to the presence of air-LFP interface, the true probing depth Δz_{LFP} is higher and can be estimated as [16,25]:

$$\Delta z_{LFP} = \Delta z \{(n_{LFP}^2 - NA^2)/(n_0^2 - NA^2)\}^{1/2} \quad (5)$$

where n_{LFP} and n_0 are refractive indexes of LFP and air respectively. Unfortunately, the formula (5) is written for a planar system, but not for a convex microparticle. The morphology of the particles under study is more complicated, so we can’t properly quantify the true depth of analysis depending on the refractive index. Another problem is the proper quantification of the refractive index, which is very important for probing depth estimation. We doubt that all the particles have the same relative permittivity

and permeability. Both parameters depend on defects thus refractive index can vary from particle to particle.

All the mentioned above factors affect the quantification of the μRS probing depth, therefore we propose to estimate it for our given particulate LFP experimentally.

3.2. Experimental demonstration of excess μRS probing depth for particulate LFP

The main idea behind the experimental estimation of Raman penetration depth is schematically illustrated in Figures 1d and 1e. The model experiment implies an μRS probing of a single LFP particle on a Si substrate used as a reference underlying layer of particles. For an LFP particle whose size is less than the lateral μRS resolution *R*, the measured Raman spectrum contains two inputs from the Si substrate. One bypasses the particle from the side, while another passes through the LFP particle (Fig. 1d). For a particle whose size is greater than *R*, there is only one input from the underneath Si substrate – the one that passed through the LFP particle (Fig. 1e). And the main point of this model experiment is to analyze how the response from the Si substrate will decrease with the growth of LFP particles – whether it will fall below the level of instrumental noise or not.

The dominant Raman bands for Si and LFP do not overlap (Fig. 2a), which makes it easy to distinguish between inputs from the top LFP particle and the underlying Si substrate. The main characteristic Raman band of Si is located at about 520 cm^{-1} [26], while the dominant characteristic band of LFP is located at about 950 cm^{-1} [27]. This allows us to introduce a quantitative parameter to estimate the Raman probing depth. In this work, we use the relative Raman intensity of the Si substrate $I_{Si\ relative}$, defined as the intensity of the main Si band of substrate $I_{Si(520)}$ divided by the intensity of the main LFP band $I_{LFP(950)}$:

$$I_{Si\ relative} = I_{Si(520)} / I_{LFP(950)} = I_{Si} / I_{LFP} \quad (6)$$

There is a small secondary doublet of bands above 950 cm^{-1} in the Raman spectrum of Si substrate [26] (Fig. 2b), but this does not cause problems with the estimation of I_{Si} / I_{LFP}. This overlapping becomes notable only for very small LFP particles, and even so, inputs from LFP and Si can still be resolved (Fig. 2c).

The main point was whether the Si band at 520 cm^{-1} will disappear when the height of the LFP particle will exceed the μRS probing depth Δz. We performed several series of measurements for particles with an estimated diameter of 0.37 to 7.7 μm (Fig. 3). We used two positioning approaches to find the proper I_{Si} / I_{LFP} value for each particle. Values that could be considered outliers were verified by additional measurements. The key result is that all the measured spectra for 75 LFP@Si particles contained a clear band near 520 cm^{-1}, corresponding to the Si substrate. For example, the Si(520) band is still visible in the Raman spectrum of the 2.5 μm diameter (D_{es}) particle (particle #9 in Fig. 2). Moreover, the Si band is

present not only for the transparent pristine LFP particles but also for carbon-coated LFP powder (Fig. S1).

This fact of Si band presence in all measured spectra allows us to conclude that the Raman probing depth for LFP samples can exceed several microns and deep multiparticle μRS probing (schematically illustrated by Fig. 1c) looks reasonable. The relatively great probing depth is neither surprising nor obvious. On the one hand, LFP is a transparent material, but on the other hand, the optical scheme of modern confocal microscopes should cut-off inputs from the out-of-focus volume (Fig. 4a), thus providing a theoretical vertical resolution in Δz about 1.1 μm in air [15].

An experimental verification made for a Si substrate without an LFP particle gives Δz value of 1.4 μm (Fig. S3c) larger than theoretical estimation (4) for several reasons, including confocality, the refractive index of media, surface roughness, etc. [17]. Also, please mention that this 1.4 μm value was derived from measuring the full width at half maxima. The Raman response is detectable over a range of at least 3 microns of the z-scan (Fig. S3c). This experimental verification was made for a simplified case of a planar Si substrate. The situation with an LFP particle on a Si substrate is even more complicated.

Note that the overall spatial resolution of the μRS is provided by two factors. On the way from the laser source to the object under study, the focusing of the laser beam ensures the locality of the irradiated volume (localization of “excitation”). On the way back from the sample to the spectrometer, the confocal pinhole cuts off the response from out-of-focus volume (localization of “response”). But the feature of the μRS characterization is that X-Y localization is better than Z-localization for both excitation and response.

A laser beam can be focused by a 100· lens into a spot about 1 μm in diameter in the X-Y directions [28]. But in the Z-direction, the laser radiation will be delocalized both above and below the focus, but still interacting with the matter (Fig. 4) [17]. As a result, the out-of-focus volumetric response is expected to be less intensive but at the same time generated in a larger volume. For a planar geometry of measurement, this non-localized excitation is not a problem. It is assumed that on the way back to the spectrometer, this response from the out-of-focus excitation is supposed to be cut off by a pinhole (Fig. 4a). Thus, while μRS cannot provide localization of “excitation”, it usually provides localization of “response”. The problem is that in the case of a morphologically heterogeneous particulate sample, the geometry of the laser beam pathways is much more complicated.

Along the way there, light passes through the upper air-LFP interface, travels through the LFP particle with possible inner grain boundaries, passes through the bottom LFP-air interface, air-SiO_2, and SiO_2-Si interfaces, generates a Raman signal, interacting with lattice vibrations, and repeats back, scattering at each interface. And some of these interfaces are irregular or even rough. In some system configurations, all these irregularities can dissipate response from the bulk, thereby reducing the probing depth. Alternatively, a micron-scale particle can act as a kind of lens, redirecting the “out-of-focus” response to the pinhole (Fig. 4b). In the case of solid-state synthesized LFP, the “focusing” property should vary from

particle to particle due to the unique irregular shape, but in any case, the convex shape of the particles promotes focusing rather than defocusing.

3.3. Inhomogeneity of optical properties

Our results show that the Raman probing depth cannot be determined precisely for particulate LFP samples. This statement is illustrated in Figure 5, where significant variations in optical properties are observed for two particles of approximately similar size.

Both optical images (Fig. 5a-c) and Raman images (Fig. 5d,f) demonstrate that particle #58 is more transparent than particle #57. For particle #58, the LFP band at 950 cm^{-1} is almost 7 times less intense than the Si band at about 520 cm^{-1} while for particle #57 it is 3.5 times more intense. This means that particle #58 transmits the response from the bottom substrate 24 times better than particle #57. This difference is also illustrated in Fig. 3 (inset) by the corresponding variation of the I_{Si}/I_{LFP} parameter. The more transparent particle #58 is marked with white filling, while a less transparent particle #57 is marked with dark gray filling. Fig. 3 is very illustrative, especially in the log-log scale (Fig. 3, inset). It should be noted that the obtained I_{Si}/I_{LFP} values on the log-log plot are not evenly spaced, we cannot draw a fitting line and claim that this I_{Si}/I_{LFP} value corresponds to this value of D_{es}. For almost any particle size, one can find a pair with the same diameter but ten times smaller I_{Si}/I_{LFP}. For larger particles, the variation of this parameter exceeds two orders of magnitude (see, for example, the size range of 2-5 μm in Fig. 3). Since I_{Si}/I_{LFP} somehow characterizes local optical transparency, Fig. 3 illustrates a significant variation of the local optical properties.

How to explain such an optical heterogeneity of particulate LFP? The above-suggested “focusing” property of a convex LFP particle hardly can be the only reason. The difference by an order of magnitude is too large to be explained only by geometric optics. An analysis of the results obtained allows us to propose two physicochemical explanations.

Local inhomogeneity of optical properties can be caused by the spatial inhomogeneity of defects and impurities. Usually, transparency is measured by integral methods, and the question is whether the optical properties are the same at each point or they can vary from particle to particle. Earlier we demonstrated the spatial inhomogeneity of defects in poorly conducting $Li_4Ti_5O_{12}$ using both similar single-particle approach [29] and statistical RS [30]. LFP is also poorly conducting material, thus impurities and defects can greatly increase its conductivity [20,31,32]. But contrary to opaque $Li_4Ti_5O_{12}$, LFP is transparent. Even a small variation of defects concentration can notably change the relative permittivity and permeability thus changing the optical properties and making one particle less transparent than another due to the excess of free charge carriers. Such a variation of the optical properties can explain the anomalous kinetics of decomposition of the LFP powder [33]. For similar excitation laser power, some measurements induced the degradation in some parts of the sample, but not in others. We can assume that the decomposition kinetics was initiated in particles with a higher concentration of defects (with lower transmittance and higher absorbance).

Another version supposes a resonance effect. The scattering of electromagnetic wave by a spherical particle on a substrate is a typical problem in theoretical physics known for over a century [34] and often called Mie scattering or Mie resonance [35–37]. By controlling the geometry of scattering objects, one can cloak them from electromagnetic fields [36] and create metamaterials with negative permeability [35]. For the situation shown in Fig. 5, the drastic variation of the optical properties for the particles of approximately the same size can be explained either by a variation of its shape (particle #58 is squarer, while particle #57 is more rounded) or by the presence or absence of a core-shell structure. If one particle has a higher concentration of defects on its surface, it can have different optical properties, even if the concentration of defects in the bulk of the particles is the same. Although Mie scattering/resonance for LFP has not been studied, a similar amplification effect has been observed and described for poorly conducting SiO_2-TiO_2 core-shell particles [38]. The increase in the signal intensity by a factor of 2.5 with an increase in the number of layers (from 1 to ≥5) was explained by the author as “enhancement without plasmons” due to the “self-resonator” geometry. We can additionally suppose that the Mie scattering/resonance effect allowed to obtain a Raman response from deeper layers. The SiO_2-TiO_2 core-shell particles size was about 2 microns, so overall Raman penetration depth could have reached ten microns for a five-layer configuration.

Besides, Mie scattering can explain the presence of a characteristic Si band at the Raman spectra of the LFP/C composite powder, considered as opaque (Fig. S1). The Si substrate is supposed to be covered by several layers of LFP particles with conductive carbon coating. The screening efficiency of the carbon shell is demonstrated by the very weak LFP band at about 950 cm^{-1}. Although this thin carbon layer can screen the LFP core just a few nanometers below, it cannot screen the Si substrate under all the layers of the LFP/C particles. It would be reasonable to assume that, due to a certain combination of particle size and core-shell geometry, highly conductive powders became relatively transparent.

This article is solely experimental and methodological, not theoretical. To confirm or refute our assumption about the Mie scattering behind a significant variation of the I_{Si}/I_{LFP} parameter, it would be necessary to perform a series of theoretical calculations or computer simulations. Nevertheless, here we propose to use a qualitative rather than a quantitative formulation of the Raman penetration depth in the particulate LFP. The significant divergence of both shapes and conductivities of individual particles results in the variation of their optical properties even for a pristine LFP sample.

In the case of carbon-coated LFP, the situation could be even more difficult. The morphology and structure of the carbon coating can vary greatly within a sample, depending on the synthesis method [39,40]. The deposition of carbon causes the formation of a defect in the electrode material and makes their distribution more spatially inhomogeneous [41]. As a result, the estimation of the Raman probing depth in the LFP/C composite will require a series of measurements with statistical analysis of the obtained results.

3.4. Lateral submicron resolution and superficial probing

The lateral resolution of μRS probing was estimated by analyzing μRS maps of the LFP@Si particles. SEM, optical microscopy, and Raman microscopy (μRS maps or scans) images are displayed in Fig. 6. μRS maps for the LFP particles (Fig. 6d, 6h, 6m) and the Si substrate (Fig. 6c, 6g, 6l) are plotted from the same scan by the corresponding major band intensity – 540 cm^{-1} for Si and 950 cm^{-1} for LFP.

Submicron spatial resolution of μRS for LFP@Si particles is somehow confirmed by resolving two adjacent LFP particles in Fig. 6m. Besides that, the “shadow” area around particle #58 (Fig. 5d and 6c) at Si substrate maps is about 0.5 μm, the one around particle #65 (Fig. 6l) is even thinner. This comply with the theoretically calculated lateral resolution 0.55 μm (R=0.61·λ/NA for λ = 0.633 and NA= 0.75) [15]. Experimental verification of the lateral resolution by the “scanning-knife” method [17,28] is close to this value (about 0.64 μm, more details see at Fig. S3a,b). As a result, it can be concluded that, in contrast to the vertical resolution, the lateral one didn’t suffer much from the complex geometry of the sample under study.

Dark “shadow” belts can be seen around most of the scanned LFP particles at Si(520) amplitude maps (Fig. 6c, 6g, and 6l), but not all (Fig. 5f). The width of this “belt” can vary, but such a shadowed border around particle is quite common. This feature can be explained either by peculiarities of Mie scattering or by the fact that steep parts of microparticles can scatter laser radiation both on the way forward (“excitation”) and backward (“response”). This double scattering significantly decreases the μRS response from the underlying substrate.

This blocking of the response at a particle’s edge is another illustration of the problem with quantifying the μRS probing depth. But, unlike an increase in the probing depth due to Mie scattering or focusing effect on microparticles, this peculiarity can result in a decrease in the probing depth. Any powder sample contains pores. A pore is a volume at the edge of two or more particles. Thus these pores can trap or block the Raman response from underlying layers. Moreover, analysis of maps for the Si substrate demonstrates that these pores can block the response more effectively than particles (Fig. 6c, 6g, 6l). This feature can indirectly restrict the vertical resolution (probing depth) from micron to submicron scale, at least for particulate systems with the core-shell geometry (for example, particles with more structured core/bulk and less structured shell).

Let us consider the μRS probing in a relatively small pore with a diameter near theoretical lateral resolution of 0.5 μm or less. Raman spectra measured in such a pore could contain responses from both upper and lower layers, but the latter one can be effectively blocked by the pore. The Raman response from the upper layer is excited not in the bulk of the particle, but only in its outer shell (Fig. 4d). Thus, the probing laser radiation still excites a large volume somewhere underneath, but the configuration of the object under study together with the confocal scheme localizes the response down to the submicron scale. Even though this response could be averaged over several particles surrounding this pore (Fig. 4d), this response can still be attributed to shell probing. Of course, in this case, the submicron resolution should not be described as “lateral” or “vertical”, but as “overall”. As a result, the μRS measurement in a

small pore can be attributed to superficial probing with submicron “overall” resolution/localization, schematically illustrated in Fig. 1a.

Please mention that steep parts of particles and pores may block the Raman response from the underneath layers, but not must. Our model experiment is a quasi 2D case. The probing laser beam was focused on the upper LFP particle. Further, we scanned/mapped at this Z position, so the response blocking was revealed for such a 2D scan only. This experiment matches the traditional Raman spectra measurement at the powder surface, but in the case of 3D measurement, theoretically possible for such a transparent material as LFP, the properties of pores may differ.

Further analysis of Figure 5 provides another reason why some of the measured Raman spectra can be attributed to superficial probing. As one can see, LFP particle #58 (Fig. 6a-d) is not just “transparent” for the response of the Si substrate but can even locally enhance the Si response. The Si substrate map (Fig. 5d and Fig. 6c) has two local maxima, both are located under the particle, but not aside as it would be natural to assume. One of these maxima is observed under the center of the particle, and the other under the sharp tip on the left. Moreover, a submicron particle can be mentioned above this tip. This small particle does not significantly contribute to the LFP response, but slightly increases the intensity of the Si characteristic band.

Besides, it can be noted that while the upper particle #62 has an elongated shape (Fig. 5e,f), the most intense response from the underlying Si substrate (Fig. 5g) is observed only in a certain localized region. In Fig. S2a,d, one can see four particles in a row. The relatively large μRS scan shows that they all enhance the response of the Si substrates (Fig. S2g). At the same time, two particles in Fig. S2b,e exhibit different properties: the left one enhances the response of the Si substrate, while the right one does not (Fig. S2h). For comparison, one can see a relatively transparent particle (Fig. S2c,f) without the Si substrate response enhancement (Fig. S2j). Particle #57 also shows no signs of local enhancement (compare Fig. 5f and 5d).

We think that the most natural explanation of such a peculiarity is a possible plasmon enhancement by curvatures of an LFP particle in contact with the Si substrate or near it. The solid-state synthesized LFP particles have an irregular shape. Some have nano-sized tips or sharp edges that act as a hotspot, similar to a nanoparticle used in Surface-Enhanced Raman Spectroscopy (SERS) and a tip in Tip-Enhanced Raman Spectroscopy (TERS). Of course, the studied LFP particles are not coated with silver or gold, but the presence of noble metals is not strictly necessary. Surface plasmon resonance can be observed in an oxide material, modified by doping [42] or by defect engineering [43]. LFP itself has low electronic conductivity, but doping [20], controlled off-stoichiometry [31] or the presence of Li vacancies [32] can drastically increase it. It can be assumed that the combination of defective surface of the LFP particle with the proper geometry of surface irregularities can lead to an enhancement of Raman response due to surface plasmon resonance. This enhancement is not observed for all studied particles, but it is still a common phenomenon. By the way, plasmon surface resonance can again be considered as a part of the Mie resonance for nanoscale objects.

4. Conclusions

The spatial resolution of micro-Raman spectroscopy was studied for single LFP particles deposited on a Raman-active Si substrate serving as a model of the underlying layer of particles in a powder. This study allowed us to conclude that the vertical μRS resolution for particulate systems should be described not quantitative, but qualitative, at least for the transparent LFP with inhomogeneity of shape and structure. Although the experimentally observed lateral resolution was shown to be close to theoretically estimated 0.55 μm, the probing depth is highly variable and may be greater or less than the theoretically estimated 1.1 μm.

Raman spectrum of pristine LFP powder measured with a confocal Raman microscope can contain both superficial and bulk responses. These responses can be provided by a single layer or several layers of particles. Multilayer probing (excessive probing depth) can be attributed to Mie scattering since some configurations of the particulate system can radically change the geometry of propagation of the electromagnetic wave. The variation in the shape of particles and the concentrations of defects/impurities both from one particle to another and within one particle leads to a significant inhomogeneity of the local optical properties. Superficial probing (smaller probing depth) can be explained by the blocking properties of pores and surface plasmon resonance due to nanoscale surface irregularities of particles together with increased electrical conductivity of the surface layer in some particles.

As far as Raman probing depth in a powder sample can vary from point to point, we suggest using different approaches for different tasks. For local measurement, it is better to use a single-particle measurement for a particle deposited on a Raman-inactive substrate. For an integral measurement, it is best to take a series of measurements with a low-magnification lens at various points and consider the resulting response as a value averaged over several layers.

Declarations

Acknowledgments

This work was performed within the Ministry of Science and Higher Education of the Russian Federation State Task FEUZ-2020-0054. The equipment of the Ural Center for Shared Use “Modern nanotechnology” Ural Federal University (Reg.№ 2968) was used with the financial support of the Ministry of Science and Higher Education of the Russian Federation (Project № 075-15-2021-677). Authors thank Dmitrii K. Kuznetsov for SEM imaging, as well as Vadim S. Gorshkov and Artur R. Makhmutov for providing a pristine LFP sample and Jongwoo Lim for providing a carbon-coated LFP sample. Special thanks to reviewers for a productive discussion.

Conflicts of Interest: The authors declare no conflict of interest.

References

[1] A. K. Padhi, K. S. Nanjundaswamy, C. Masquelier, S. Okada, J. B. Goodenough, *J. Electrochem. Soc.* **1997**, *144*, 1609.

[2] A. K. Padhi, J. B. Nanjundaswamy, K.S. Goodenough, *J. Electrochem. Soc.* **1997**, *144*, 1188.

[3] M. Gupta, *Can LFP technology retain its battery market share?*, **2020**.

[4] X. Hao, Y. Zhou, H. Wang, M. Ouyang, *Mitig. Adapt. Strateg. Glob. Chang.* **2020**, *25*, 329.

[5] X. Zeng, M. Li, D. Abd El-Hady, W. Alshitari, A. S. Al-Bogami, J. Lu, K. Amine, *Adv. Energy Mater.* **2019**, *9*, 1900161.

[6] D. V. Pelegov, J. Pontes, *Batteries* **2018**, *4*, 65.

[7] E. E. Ferg, F. Schuldt, J. Schmidt, *J. Power Sources* **2019**, *423*, 380.

[8] S. Maddukuri, D. Malka, M. S. Chae, Y. Elias, S. Luski, D. Aurbach, S. Maddukuri, D. Malka, M. S. Chae, Y. Elias, S. Luski, *Electrochim. Acta* **2020**, *354*, 136771.

[9] C. M. Julien, K. Zaghib, A. Mauger, M. Massot, A. Ait-Salah, M. Selmane, F. Gendron, *J. Appl. Phys.* **2006**, *100*, 063511.

[10] D. J. Gardiner, P. R. Graves, Eds., *Practical Raman Spectroscopy*, Springer Berlin Heidelberg, Berlin, Heidelberg, **1989**.

[11] R. G. Sparks, W. S. Enloe, M. A. Paesler, *Precis. Eng.* **1991**, *13*, 189.

[12] M. Ivanda, K. Furić, *Appl. Opt.* **1992**, *31*, 6371.

[13] I. De Wolf, J. Chen, M. Rasras, W. M. van Spengen, V. Simons, (Eds: R. A. Lieberman, A. K. Asundi, H. Asanuma), **1999**, pp. 239–252.

[14] A. Sarua, Hangfeng Ji, M. Kuball, M. J. Uren, T. Martin, K. P. Hilton, R. S. Balmer, *IEEE Trans. Electron Devices* **2006**, *53*, 2438.

[15] G. Gouadec, P. Colomban, *Prog. Cryst. Growth Charact. Mater.*, **2007**, *53*, 1–56.

[16] F. Foucher, G. Guimbretière, N. Bost, F. Westall, in *Raman Spectroscopy and Applications*, InTech, **2017**.

[17] F. Foucher, *J. Raman Spectrosc.* **2021**, jrs. 6230.

[18] D. J. Griffiths, R. College, *Introduction to Electrodynamics*, Prentice Hall, Upper Saddle River, New Jersey, 3rd edn., **1999**.

[19] M. Park, X. Zhang, M. Chung, G. B. Less, A. M. Sastry, *J. Power Sources* **2010**, *195*, 7904.

[20] S.-Y. Chung, J. T. Bloking, Y.-M. Chiang, *Nat. Mater.* **2002**, *1*, 123.

[21] E. J. Flores Cedeño, Development of operando diagnostics for Li-ion cathodes by Raman spectroscopy, ETH Zurich, **2019**.

[22] H. Lee, H. Yim, K.-B. Kim, J.-W. Choi, *J. Nanosci. Nanotechnol.* **2015**, *15*, 8627.

[23] A. B. Béléké, C. Faure, M. Röder, P. Hovington, U. Posset, A. Guerfi, K. Zaghib, *Mater. Sci. Eng. B* **2016**, *214*, 81.

[24] H. Lee, S. Kim, N. S. Parmar, J.-H. Song, K. Chung, K.-B. Kim, J.-W. Choi, *J. Power Sources* **2019**, *434*, 226713.

[25] N. J. Everall, *Analyst* **2010**, *135*, 2512.

[26] J. H. Parker, D. W. Feldman, M. Ashkin, *Phys. Rev.* **1967**, *155*, 712.

[27] W. Paraguassu, P. T. C. Freire, V. Lemos, S. M. Lala, L. A. Montoro, J. M. Rosolen, *J. Raman Spectrosc.* **2005**, *36*, 213.

[28] P. Hauer, J. Grand, A. Djorovic, G. R. Willmott, E. C. Le Ru, *J. Phys. Chem. C* **2016**, *120*, 21104.

[29] D. V. Pelegov, B. N. Slautin, P. S. Zelenovskiy, D. K. Kuznetsov, E. A. Kiselev, D. O. Alikin, A. L. Kholkin, V. Y. Shur, *J. Raman Spectrosc.* **2017**, *48*, 278.

[30] D. V. Pelegov, B. N. Slautin, V. S. Gorshkov, P. S. Zelenovskiy, E. A. Kiselev, A. L. Kholkin, V. Y. Shur, *J. Power Sources* **2017**, *346*, 143.

[31] B. Kang, G. Ceder, *Nature* **2009**, *458*, 190.

[32] A. Banday, M. Ali, R. Pandey, S. Murugavel, *Phys. Chem. Chem. Phys.* **2019**, *21*, 9858.

[33] A. A. Ryabin, B. N. Slautin, D. V. Pelegov, *J. Raman Spectrosc.* **2020**, *51*, 528.

[34] G. Mie, *Ann. Phys.* **1908**, *330*, 377.

[35] Q. Zhao, J. Zhou, F. Zhang, D. Lippens, *Mater. Today* **2009**, *12*, 60.

[36] J. B. Pendry, *Science (80-.).* **2006**, *312*, 1780.

[37] D. Tzarouchis, A. Sihvola, *Appl. Sci.* **2018**, *8*, 184.

[38] I. Alessandri, *J. Am. Chem. Soc.* **2013**, *135*, 5541.

[39] D. V. Pelegov, A. A. Koshkina, V. I. Pryakhina, V. S. Gorshkov, *J. Electrochem. Soc.* **2019**, *166*, A5019.

[40] D. V. Pelegov, A. A. Koshkina, B. N. Slautin, V. S. Gorshkov, *J. Raman Spectrosc.* **2019**, *50*, 1015.

[41] D. V. Pelegov, R. N. Nasara, C. Tu, S. Lin, *Phys. Chem. Chem. Phys.* **2019**, *21*, 20757.

[42] H. Yu, Y. Peng, Y. Yang, Z.-Y. Li, *npj Comput. Mater.* **2019**, *5*, 45.

[43] E. L. Runnerstrom, A. Bergerud, A. Agrawal, R. W. Johns, C. J. Dahlman, A. Singh, S. M. Selbach, D. J. Milliron, *Nano Lett.* **2016**, *16*, 3390.

Figures

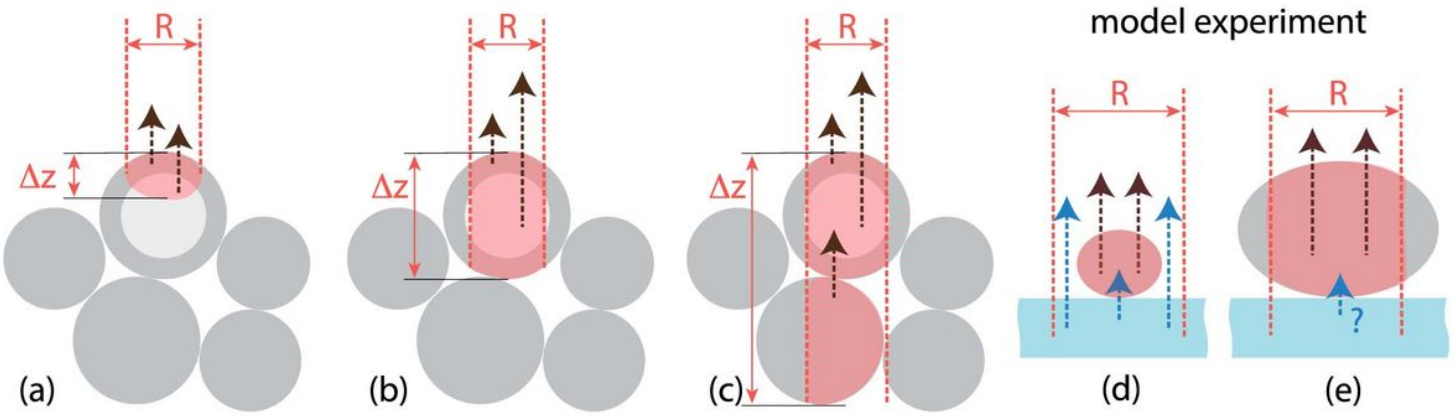

Figure 1

Schematic illustration of possible mRS probing depths for a microscale powder system (a)-(c) and a single particle on an RS-active substrate (d), (e). Powder probing by mRS: (a) superficial, (b) single-particle, and (c) deep multiparticle. LFP@Si probing is illustrated for particles (d) smaller and (e) larger than the lateral resolution *R*. The dashed red lines indicate the probing laser beam, red area shows the probed volume. The dashed arrows indicate inputs to the Raman response from different parts of the probed volume. More realistic laser beam geometry could be found further in Fig. 4.

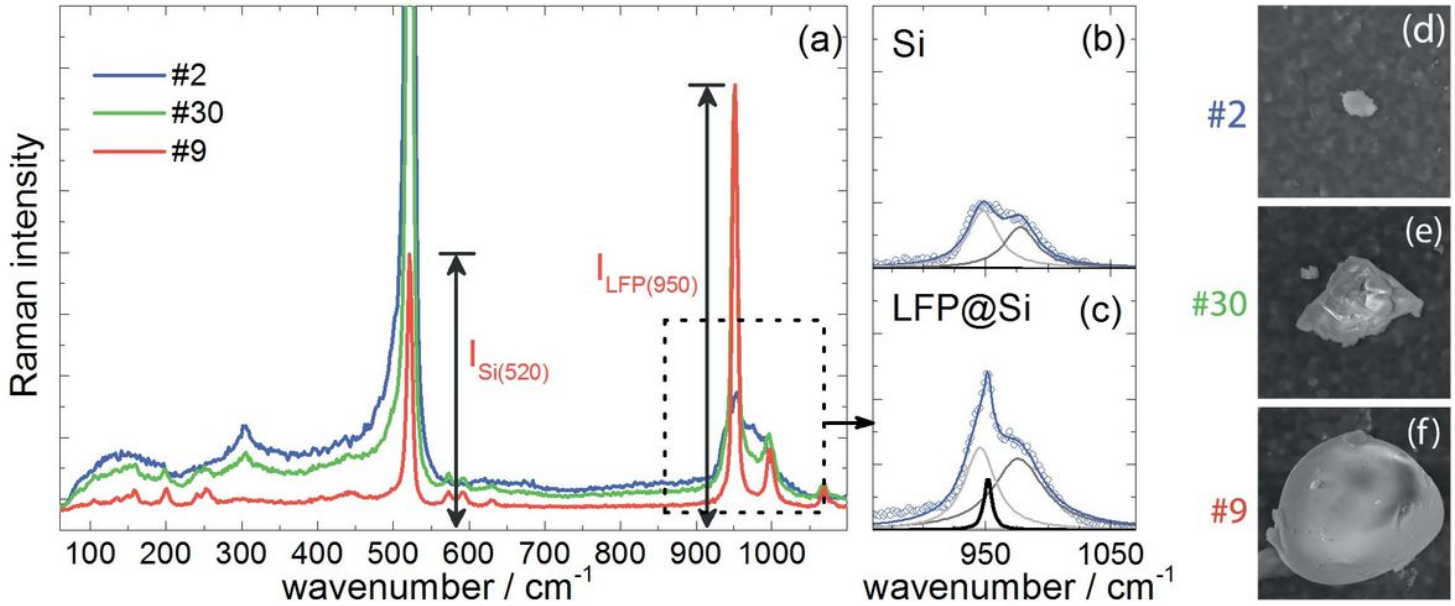

Figure 2

(a) Raman spectra of LFP@Si particles of different sizes and (d)-(f) SEM images of the corresponding particles. SEM images are 3 × 3 μm^2. Estimated particle sizes D_{es}, μm: (d) 0.44, (e) 1.4, (f) 2.5. Deconvolution of the Raman spectrum at about 950 cm^{-1}: (b) for a Si substrate without an LFP particle; (c) for small LFP@Si particle #2.

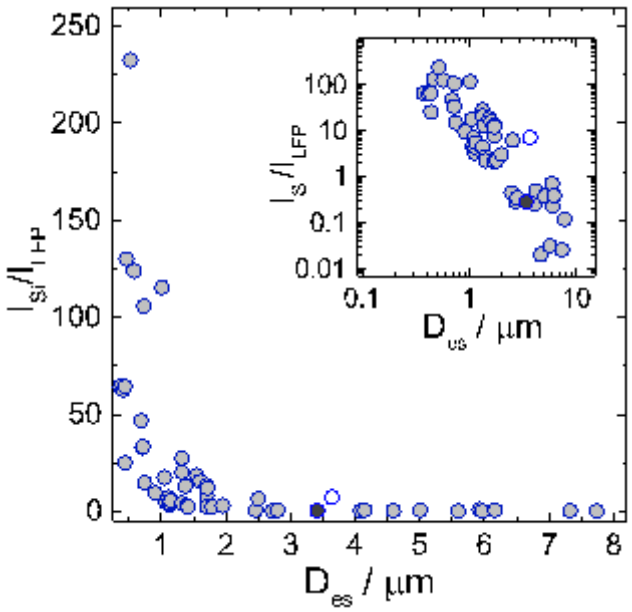

Figure 3

Dependences of the relative Raman intensity of the substrate on the estimated size D_{es} for the LFP@Si particles in linear and log-log (inset) scales. Particle #58 – white, particle #57 - dark-grey.

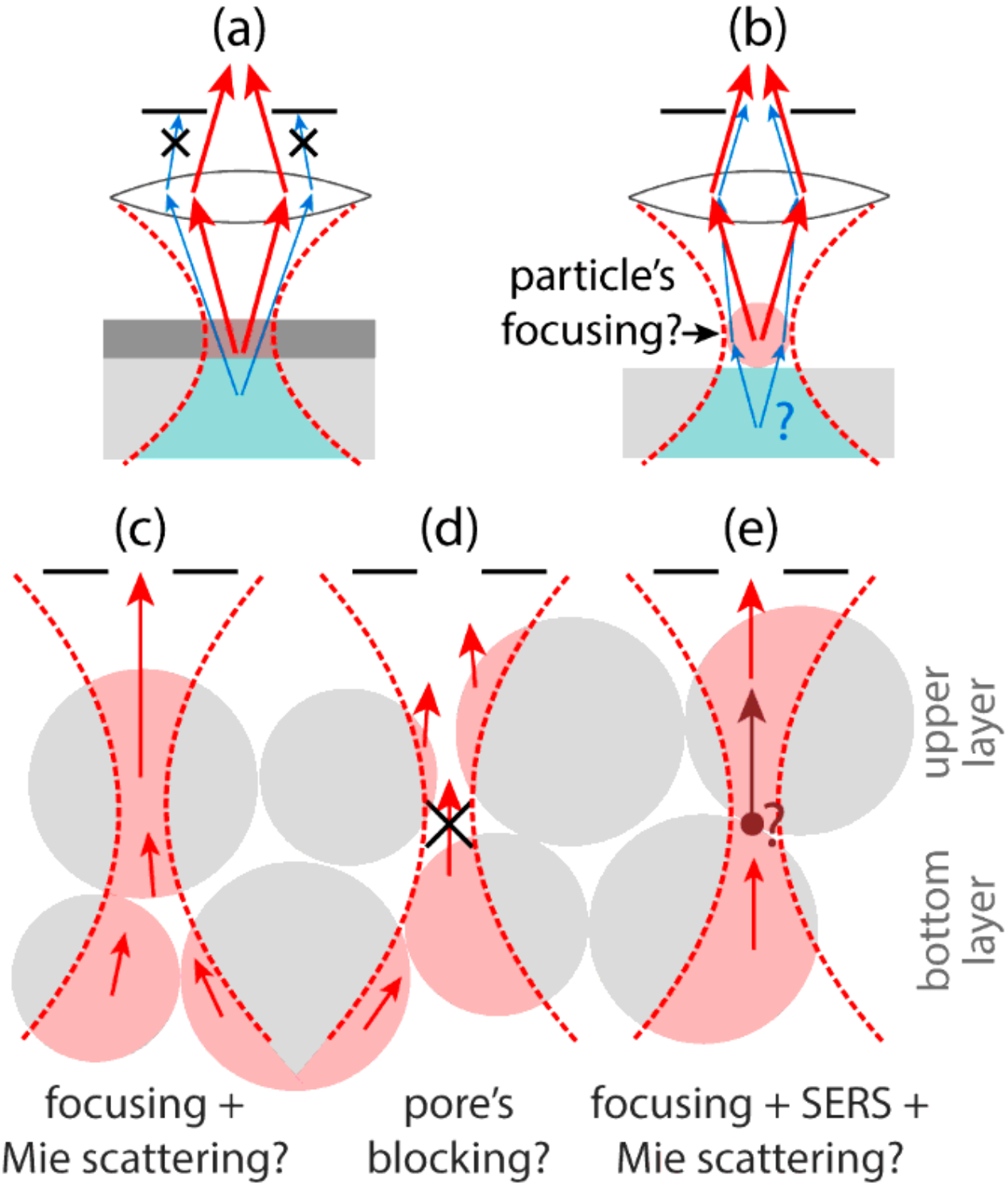

Figure 4

Schematic illustration of mRS probing for: (a) a single crystal, (b) a single particle on a Raman-active substrate, and (c)-(e) a powder sample. (c) and (e) correspond to deep multiparticle probing, (d) –

blocking of deep Raman response by pores, and (e) possible moderate enhancement due to particle curvature.

Figure 5

Comparison of the optical properties of particles #57 and #58. The red squares in the optical images (a) and (c) indicate the corresponding Raman images/maps for input from the Si substrate (d) and (f). Optical image with both particles (b) compared to SEM image of the same region at the same scale (e).

Figure 6

Comparison of SEM (a), (e), (j) and optical (b), (f), (k) images with Raman mappings for Si (c), (g), (l) and LFP (d), (h), (m). Red rectangles in optical images indicate the area of the corresponding Raman mappings. SEM images are 5 × 5 μm^2. The white scale bar width is 2 μm for optical images and 1 μm for Raman mappings.

Supplementary Files

This is a list of supplementary files associated with this preprint. Click to download.

- RyabinPelegovmRSresolutioneSM.docx
- graphicalabstractnew.tif